DOI: 10.26599/FSHW.2026.9251290

Contents lists available at SciOpen

Food Science and Human Wellness

journal homepage: https://www.sciopen.com/journal/2097-0765

China Food Publishing Co.

Dietary Polyphenol Oxyresveratrol Ameliorates Alcohol-Associated Liver Disease through Dual Regulation of Hepatic AMPK/SIRT1 Pathway and Gut +Microbiota

Zexi Tian[a,b,1], Rong Yuan[a,b,1], Yingbo Liu[a,b], Li Guo[a,b], Congjie Yan[a,b], Weidong Wang[a,b,*], Zenggen Liu[a,b,c,*]

[a] *School of Pharmacy, Hubei University of Chinese Medicine, Wuhan, 430065, China*

[b] *Hubei Shizhen Laboratory, Hubei University of Chinese Medicine, Wuhan, 430065, China*

[c] *Center of Traditional Chinese Medicine Modernization for Liver Diseases, Hubei University of Chinese Medicine, Wuhan, 430065, China*

ABSTRACT: Alcohol-associated liver disease (ALD) represents a major global health burden, underscoring the urgent need for multi-target therapeutic approaches derived from dietary sources. Oxyresveratrol (OT), a natural polyphenol abundantly present in mulberries and grapes, possesses potent antioxidant properties; however, its comprehensive mechanisms of protection against ALD remain inadequately elucidated. This study aimed to investigate the hepatoprotective effects of OT via the dual modulation of the hepatic adenosine monophosphate-activated protein kinase/sirtuin 1(AMPK/SIRT1) signaling pathway and gut microbiota remodeling. *In vitro*, OT pretreatment significantly attenuated ethanol-induced oxidative stress and inflammatory responses in HepG2 cells. *In vivo*, OT administration markedly ameliorated alcohol-induced liver injury in C57BL/6J mice, as indicated by reduced serum ALT and AST levels, improved lipid metabolism, and suppression of key pro-inflammatory cytokines tumor necrosis factor-α (TNF-α), interleukin-1β (IL-1β), interleukin-6 (IL-6). Proteomic analysis demonstrated that OT activates AMPK/SIRT1 signaling, resulting in the upregulation of downstream targets peroxisome proliferator-activated receptor γ (PPARγ) and carnitine palmitoyltransferase 1α (CPT1α), while concurrently suppressing perilipin 2 (Plin2) and nuclear factor-κB (NF-κB) activation. Notably, OT restored gut microbiota diversity by enriching short-chain fatty acid (SCFA)-producing genera such as Lachnospiraceae, and elevated SCFAs levels in cecal and colonic contents. These microbial changes were correlated with enhanced gut-liver axis function. Collectively, our findings indicate that OT alleviates ALD through simultaneous targeting of hepatic metabolic pathways and gut microbial ecology, highlighting its potential as a effective dietary intervention for ALD. This study provides a solid theoretical foundation for the development of OT as a multi-target therapeutic agent, underscoring its translational value in functional food and pharmacological applications.

Keywords: Oxyresveratrol; Alcohol-associated liver disease; AMPK/SIRT1; Gut microbiota

1. Introduction

Alcohol-associated liver disease (ALD) represents a spectrum of hepatic disorders caused by chronic excessive alcohol consumption, progressing from simple steatosis and alcoholic hepatitis to fibrosis, cirrhosis,

[1] Co-first authors.
***Corresponding author**
wwd315@hbucm.edu.cn (W.D. Wang);
3370@hbucm.edu.cn (Z.G. Liu)

Received 8 December 2025
Received in revised from 5 February 2026
Accepted 11 May 2026

and even hepatocellular carcinoma[1,2]. Currently, alcohol abstinence remains the most effective intervention for ALD, while conventional pharmacotherapies such as corticosteroids offer only limited symptomatic relief without reversing disease progression[3,4]. Consequently, developing multi-target therapeutic agents with low toxicity has become a major research focus.

Natural products have garnered increasing attention for their potential in ALD management due to their multi-pathway synergistic effects and favorable safety profiles. Compounds such as silymarin and lentinan have been developed as functional foods or adjunctive therapies[5,6]. Among these, OT a hydroxylated derivative of resveratrol characterized as a naturally occurring stilbene polyphenol (trans-2,4,3',5'-tetrahydroxystilbene) found in plants such as mulberries, grapes, and peanuts, has emerged as a promising candidate owing to its enhanced antioxidant activity[7,8]. While resveratrol is well known for its strong hepatoprotective activity, its derivative, OT possesses an additional hydroxyl group. This structural modification endows OT with better water solubility, superior oral bioavailability, and more potent antioxidant capacity than resveratrol. Mechanistically, OT exhibits distinct advantages in free radical scavenging and specific signaling modulation[9]. Structurally, OT possesses an additional hydroxyl group at the 2'-position of the stilbene skeleton, which extends the conjugate system and augments its free radical-scavenging capacity and ability to activate the nuclear factor erythroid 2-related factor 2 (Nrf2) antioxidant pathway[10]. Previous studies have demonstrated that OT alleviates liver fibrosis by downregulating the expression of transforming growth factor-β1 (TGF-β1), phosphorylated Smad1/2 (p-Smad1/2), and phosphorylated extracellular signal-regulated kinase 1/2 (p-ERK1/2), thereby inhibiting hepatic stellate cell activation[11,12,13]. Furthermore, OT has been shown to modulate gut microbiota balance, influencing liver metabolism and inflammation via the "gut-liver axis"[14,15,16].

The AMPK/SIRT1 signaling axis has been identified as a central regulator of lipid metabolism and inflammatory responses in ALD pathogenesis[17,18]. Ethanol consumption inhibits AMPK activity, impairing fatty acid oxidation and promoting lipid accumulation, while concurrently reducing SIRT1 expression, which exacerbates oxidative stress and the release of pro-inflammatory cytokines such as TNF-α and IL-6[19]. Activation of the AMPK/SIRT1 pathway has been shown to significantly ameliorate ethanol-induced hepatocyte apoptosis and steatosis[20,21]. PPARγ, a downstream target of SIRT1, plays a critical role in promoting fatty acid β-oxidation and suppressing lipogenesis when activated[22]. Moreover, emerging evidence highlights the crucial role of gut microbiota dysbiosis in ALD progression. Alcohol and its metabolites disrupt intestinal barrier integrity, facilitating the translocation of gut-derived endotoxins to the liver, where they activate Kupffer cells and trigger inflammatory cascades[23,24]. SCFAs, key metabolites produced by gut microbiota[25], are directly associated with hepatoprotective effects when their levels are restored[26,27].

This study aims to validate the efficacy of OT against ALD through *in vivo* and *in vitro* experiments, and to thoroughly investigate its underlying mechanisms involving the AMPK/SIRT1 signaling axis and gut

microbiota reconstruction. The findings are expected to provide a theoretical foundation for developing OT as a candidate therapeutic agent for ALD.

2. Materials and methods

2.1. Materials

OT (98%, S25554) and silybin (98%, V97777) were purchased from Shanghai Yuanye Biotechnology Co., Ltd. (Shanghai, China). Reagents (ethanol, methanol, acetic acid, etc.) were obtained From Sinopharm Chemical Reagent Co., Ltd. Palmitic acid (PA, HY-N0830), Oleic acid (OA, HY-N1446) and Selisistat (EX-527, HY-15452) were purchased from MedChemExpress (Monmouth Junction, NJ,USA). Sodium butyrate (Na B, 303410) was purchased from Sigma-Aldrich (St. Louis, MO,USA). Lieber-DeCarli control liquid diet and alcoholic liquid diet were purchased from Xiaosu Youtai Biotechnology Co. (Beijing,China). Enzyme-linked immunosorbent assay (ELISA) TNF-α detection kit, IL-1β detection kit, and IL-6 detection kit; Hematoxylin staining solution, eosin staining solution,oil red O staining solution, malondialdehyde (MDA) and superoxide dismutase (SOD) assay kits were purchased from Beijing Solarbio Science&Technology Co.,Ltd (Beijing,China). The alanine aminotransferase (ALT), aspartate aminotransferase (AST), Total cholesterol (TC) and Triglyceride (TG) assay kits were purchased from Nanjing Jiancheng Institute of Bioengineering (Nanjing, China). Albumin BovineV (BSA) purchased from Beijing Biotopped Technology Co. (Beijing,China). The antibodies used in this study are as follows: Anti-ORP8 (AB228990, Abcam, UK), anti-NF-κB, (AB16502, Abcam, UK), anti-p-NF-κB (AB76302, Abcam, UK), anti-AMPK (10929-2-AP, PTG, China), anti-P-AMPK (AF3423, Affinity, China), anti-Plin2 (15294-1- AP, PTG, China), anti-PPARγ (16643-1-AP, PTG, China), anti-SIRT1 (DF6033, Affinity, China), anti-ATGL (55190-1-AP, PTG, China), anti-CPT1α (15184-1-AP, PTG, China), anti-Adiponectin (21613-1-AP, PTG, China), anti-Nrf2 (16396-1-AP, PTG, China), and anti-β-actin (20536-1-AP, PTG, China), HRP-Goat Anti-Rabbit Recombinant Secondary Antibody (H+L) (RGAR001,PTG, China).

2.2. Cell culture and cell viability assay

HepG2 cells were obtained from the cell bank of Wuhan Pricella Biotechnology Co. All cells were cultured in 89% Minimum Essential Medium with NEAA (PM150410, Wuhan Pricella Biotechnology Co.), 10% foetal bovine serum (164210, Wuhan Pricella Biotechnology Co.) and 1% penicillin-streptomycin (PB180120, Wuhan Pricella Biotechnology Co.) at 37℃ in a humidified incubator containing 5% CO2. Briefly, HepG2 cells were seeded in 96-well plates at a density of 5×10^3 cells per well with a working volume of 100 μL per well. For subsequent experiments, cells were seeded in 96-well plates and 6-well plates at densities of 5×10^3 cells per well and 2 × 10^5 cells per well, respectively, with working volumes of 100 μL per well (96-well plates) and 2 mL per well (6-well plates). After HepG2 cells had adhered, they were treated separately with different concentrations of OT, Na B, or EX-527 for 24 h. Subsequently, Cell Counting Kit-8 (CCK-8; MA0218, Dalian Meilun Biotechnology Co., Ltd.) reagent was added, and the cells were incubated at 37℃ for 2 h. Absorbance at 450 nm was measured using a full-wavelength microplate reader (KAIAO,

China) to evaluate cell viability. After attachment, the cells were exposed to medium containing 100mmol/L ethanol and free fatty acids (FFA) for 24 h to establish the cell injury model. To minimize the effect of ethanol volatilization and maintain relatively stable exposure conditions, after the initial 24 h incubation, the culture medium was discarded and replaced with freshly prepared medium containing 100 mmol/L ethanol at the same concentration, FFA, and different concentrations of OT for an additional 24 h treatment. In the inhibitor experiments, cells were first pretreated with EX-527 for 1 hour, followed by co-culture with OT for 3 hours. The medium was then replaced with fresh medium containing 100 mmol/L ethanol while maintaining the concentrations of EX-527 and OT, and biochemical analysis was performed after 24 hours of further culture. For biochemical assays, cells were collected and lysed, and ALT, AST, MDA, and SOD levels were measured in the cell lysates according to the manufacturer's instructions.

2.3. Animal models and experimental design

Male C57BL/6J mice (SPF grade, 6-7 weeks, 20 ± 2g) were purchased from Wuhan Chunyuhong Experimental Animal Feed Co., Ltd. Mice were acclimatised for one week in a 25 ℃ SPF environment with unrestricted access to standard rodent food and water. Animal procedures followed the Guide for the Care and Use of Laboratory Animals to ensure that pain and suffering were minimized (NWIPB-CAS IAEC-20240185). Then, mice were randomly divided into five groups (n = 6): control group, model group, silybin group, OT low-dose group (OT-L), and OT high-dose group (OT-H). Except for the control group, all other groups were fed a Lieber-DeCarli ethanol liquid diet, in which ethanol accounted for approximately 36% of total caloric intake, to establish the ALD model. The ethanol-containing liquid diet was freshly prepared according to standard protocols. Mice underwent 7 days adaptation period before ethanol feeding. After six weeks of Lieber-DeCarli ethanol liquid diet feeding, mice in the treatment groups continued to receive the ethanol liquid diet during weeks 7–8, while being simultaneously administered silybin (50 mg/kg), OT (50 mg/kg), or OT (100 mg/kg) by oral gavage once daily. To further mimic acute binge drinking, mice received an oral gavage of ethanol at a dose of 5 g/kg body weight (approximately 31.5% v/v ethanol solution) at the end of the feeding period. Mice in the control and model groups received an equivalent volume of 0.5% carboxymethylcellulose sodium (CMC-Na) solution. At the end of the treatment period, blood samples were collected, and all animals were euthanized. Serum, liver, and cecal and colonic contents were harvested for subsequent analyses.

2.4. Measurement of inflammatory and oxidative stress factors and liver function indicators

Whole blood from mice was allowed to stand at room temperature for 4 h, then centrifuged twice at 3000 rpm for 10 min each at 4℃. The supernatant was collected to obtain mouse serum. Serum levels of inflammatory factors (TNF-α, IL-1β, and IL-6) were measured using ELISA kits. Biochemical parameters, including ALT, AST, TG and TC were quantified using the respective commercial kits.

2.5. Histopathological analyses

For Hematoxylin and Eosin (H&E) Staining, the fixed liver tissue was dehydrated using a gradient ethanol series, embedded in paraffin, and sectioned into 5 μmol/Lol/L serial slices. The sections were then dewaxed, rehydrated, and stained with hematoxylin and eosin. After staining, the sections were dehydrated with ethanol, cleared with xylene, and mounted with neutral gum. The Oil Red O working solution was prepared by mixing saturated staining solution with distilled water in a 6:4 ratio, and allowed to stand at 4℃ overnight. The solution was then filtered, and filtered again after standing for 24 h at 4℃. sections were stained with Oil Red O and fixed at room temperature for 15 min, followed by thorough washing. Staining was performed in the dark for 8-10 min. The sections were subsequently differentiated in 60% isopropanol, rinsed with distilled water, and restained with hematoxylin for 3-5 min to restore the blue coloration. After sealing with glycerol gelatin, the liver tissue structure and lipid deposition in liver cells were observed under a microscope, and images were captured for analysis.

2.6. Immunofluorescence (IF) analysis

Fresh liver tissue was fixed with 4% paraformaldehyde, embedded, and sectioned. The sections were blocked with 2% goat serum and incubated overnight at 4℃ with primary antibodies against OSBP-Related Protein 8 (ORP8, 1:500), Adipose triglyceride lipase (ATGL, 1:200), and Perilipin 2 (Plin2, 1:600). After washing with PBS, the sections were incubated with a fluorescent secondary antibody for 1 h under light-avoiding conditions. The sections were then washed three times with PBS. Nuclei were stained by adding 1 μg/mL DAPI (prepared in PBS) for 5 min, followed by rinsing in PBS and blocking. Images were captured at 20× magnification using a fluorescence microscope (Nikon, Nikon Eclipse C1), and data were analyzed using ImageJ software (NIH USA).

2.7. RNA extraction and RT-PCR analysis

All reagents used in this section were purchased from Servicebio (Wuhan, China). Total RNA was extracted from liver tissues using TRIzol reagent and cDNA was obtained by reverse transcription of RNA samples using RT reagent. $^{\triangle\triangle}$ CT assay was used to detect the gene expression of IL-1β, TNF α and IL-6. The primer sequences used in the experiment are provided in the supplementary materials (Table S1). β-actin was used as an endogenous control. The primers used were provided by WUHAN Genecreate Bio logical Engineering Co., Ltd. (Wuhan, China).

2.8. Proteomic analysis

Proteomic profiling of liver tissue was performed by the technology of Paysonol Co., Ltd. (Shanghai, China) using Astral-DIA technology. Data processing and statistical evaluation were performed using the Majorbio cloud platform and R programming. Total proteins were extracted from liver tissues, and after the concentration was determined by BCA method, trypsin digestion was performed to generate peptides, which were purified and desalted and lyophilised on a C18 column. Quality control was performed prior to LC-MS analysis, and the peptides were separated using a high-resolution mass spectrometer and a reversed-phase C18

column, and the DIA data were collected in the range of 350-1800 m/z. Proteins were quantified by Spectronaut software (FDR < 1%) using a library-free method. Differentially expressed proteins (DEPs) with a screening criterion of |log2FC|≥1 and corrected P<0.05 were analysed for KEGG enrichment (FDR-corrected).

2.9. 16S. rRNA sequencing and analysis

For 16S rRNA sequencing, cecum and colon contents were collected from each group (n=3). DNA was extracted from the samples using commercially available kits (OmegaBio-tek, Norcross,GA, USA). DNA integrity and purity were assessed by 1.2% agarose gel electrophoresis and NanoDrop ND-1000 spectrophotometry, and DNA was quantified using Nanodrop. The V4 region of 16S rDNA was amplified with index primers, and sequencing libraries were prepared using Illumina's TruSeq Nano DNA LT Library Prep Kit. Sequencing was performed on an Illumina NovaSeq 6000 system (PE250 mode, SP kit V1.5). Raw data were processed by tQIIME2 dada2 analysis process/Vsearch software to calculate the hold. Raw sequencing data were spliced according to overlap relationships, and samples were differentiated, quality controlled and quality filtered, followed by OTU clustering and species annotation, α-diversity, β-diversity, cluster testing, and species taxonomic composition analysis.

2.10. Measurement of SCFAs

An appropriate amount of cecal and colonic contents was mixed with 500 μL of ultrapure water, homogenised at 70 Hz for 60 s and centrifuged at 12,000 rpm for 10 min at 4℃. An aliquot of 200 μL of the supernatant was transferred into a 1.5 mL tube and mixed with 100 μL of 15% phosphoric acid, 20 μL of 375 μg/mL 4-methylvaleric acid solution as the internal standard, and 280 μL of ether. and homogenised for 1 min and centrifuged at 4℃ 12000 rpm for 10 min. The supernatant was taken for GC-MS analysis. GC-MS analyses were performed on a Thermo Trace 1310 (Thermo Fisher Scientific, USA) gas phase system and a Thermo ISQ LT mass spectrometer (Thermo Fisher Scientific, USA) with an ionisation energy of 70 eV in the electron impact mode and a scanning range between 30 and 600 m/z. SCFAs content was quantified using external standards.

2.11. Western blotting

Liver tissue was homogenized in RIPA lysis buffer, phosphorylated protease inhibitors A, B, and PMSF (100:1:1:1). All samples were centrifuged at 13,500 rpm for 15 min at 4℃ and the supernatant was collected.Total protein was detected using BCA protein assay kits (Beyotime,Shanghai, China). The samples were separated via sodium dodecyl sulfate-polyacrylamide gel electrophoresis (epizyme, Shanghai, China), and then the proteins were transferred onto PVDF membranes (Millipore, Massachusetts, USA). The membranes were blocked with 5% nonfat milk or 5% BSA (for phosphorylated proteins) for 2 h at room temperature. The membranes were then incubated overnight at 4℃ with primary antibodies at the following dilutions:ORP8 (1:10000), Plin2 (1:8000), ATGL (1:20000), Adiponectin (1:1000), AMPK (1:20000),

p-AMPK (1:1000), SIRT1 (1:1000), PPARγ (1:3000), CPT1α (1:20000), NF-κB (1:2000), p-NF-κB (1:1000), β-actin (1:6000), Nrf2 (1:6000). The membranes were washed with TBST and incubated with the corresponding secondary antibody (1:10000) for 2 h. Target bands were detected using ECL luminescent solution (Solarbio, Beijing, China). All Western blot experiments were performed in at least three independent biological replicates. Band intensities were quantified using ImageJ software and normalized to β-actin.

2.12. Statistical analysis

Statistical analysis was performed using the Prism version 10.4 GraphPad Software (San Diego, CA, USA). Statistical analysis was conducted based on one-way ANOVA. Values are expressed as mean ± standard deviation (SD). A P value of < 0.05 was considered statistically significant. For Spearman correlation analysis between gut microbiota and SCFAs, p-values were adjusted for multiple comparisons using the Benjamini–Hochberg false discovery rate (FDR) method. Correlations with adjusted p-values (FDR < 0.05) were considered statistically significant.

3. Results

3.1. Protective Effect of OT on Alcohol-Induced Injury in HepG2 Cells

To determine the appropriate OT concentrations for subsequent *in vitro* experiments, we first performed a cell viability assay in HepG2 cells. As shown in Fig. 1B, OT treatment at concentrations ranging from 20 to 100 μmol/Lol/L did not cause significant cytotoxicity, indicating that this concentration range was well tolerated and could be used safely in the following experiments. We found that OT dose-dependently attenuated the abnormal elevation of ALT and AST activities in alcohol-exposed HepG2 cells. In addition, OT significantly alleviated oxidative stress, as evidenced by decreased MDA levels and increased SOD activity (Fig. 1C–F). These findings suggest that OT exerts a protective effect against alcohol-induced hepatocellular injury.

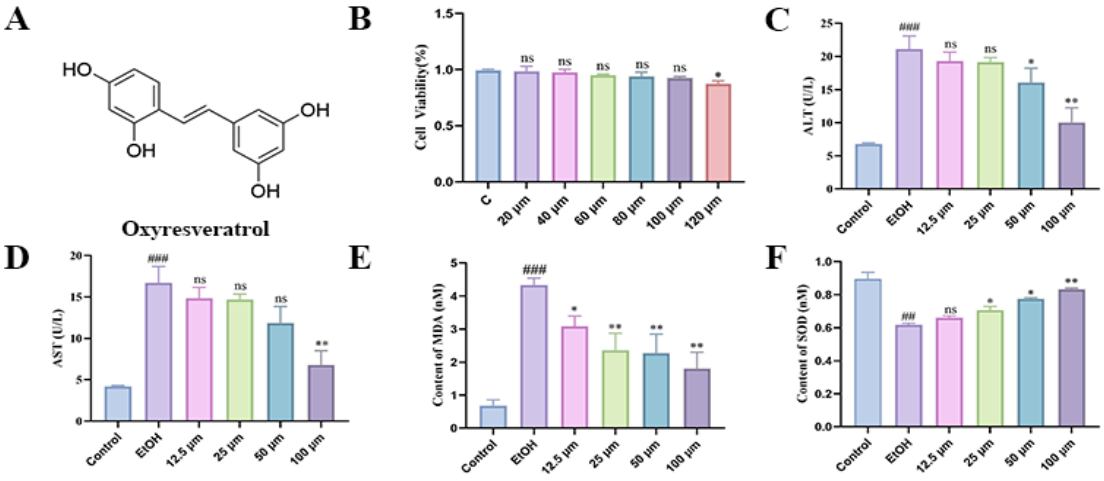


Figure 1. Preliminary Evaluation of OT's Anti-ALD Activity. (A) Structural formula of OT. (B) Effects of different concentrations of OT on the viability of HepG2 cells. (C,D) Effects of OT treatment on ALT and AST activities in HepG2 cells. (E,F) Effects of OT treatment on MDA and SOD activities in HepG2 cells. Data were presented as means ± SD. Statistical significance was determined using one-way ANOVA. (*$P < 0.05$, **$P < 0.01$ compared to the model group; #$P < 0.05$, ##$P < 0.01$, ###$P < 0.001$ compared to the control group, n = 6)

3.2. The therapeutic effect of OT on ALD

In the animal study, a mouse model of ALD was established using the Lieber-DeCarli ethanol liquid diet (Fig. 2A). After six weeks of ethanol feeding, mice received oral administration of OT during weeks 7-8. The OT treatments (100 mg/kg and 50 mg/kg) significantly attenuated ethanol-induced body weight loss and elevated liver index (liver weight/body weight) compared to the ethanol-only model group (Fig. 2B-C). As expected, serum levels of AST and ALT were significantly elevated in the model group after 8 weeks of ethanol exposure, whereas OT treatment markedly reduced both enzymes (Fig. 2D-E). Similarly, OT administration significantly suppressed ethanol-induced increases in serum TG and TC levels (Fig. 2F-G). Moreover, OT treatment significantly reduced plasma levels of the proinflammatory cytokines IL-1β, TNF-α, and IL-6 (Fig. 2H-J), consistent with the hepatic mRNA expression patterns revealed by RT-PCR (Fig. 2K-M), further confirming OT's anti-inflammatory efficacy.

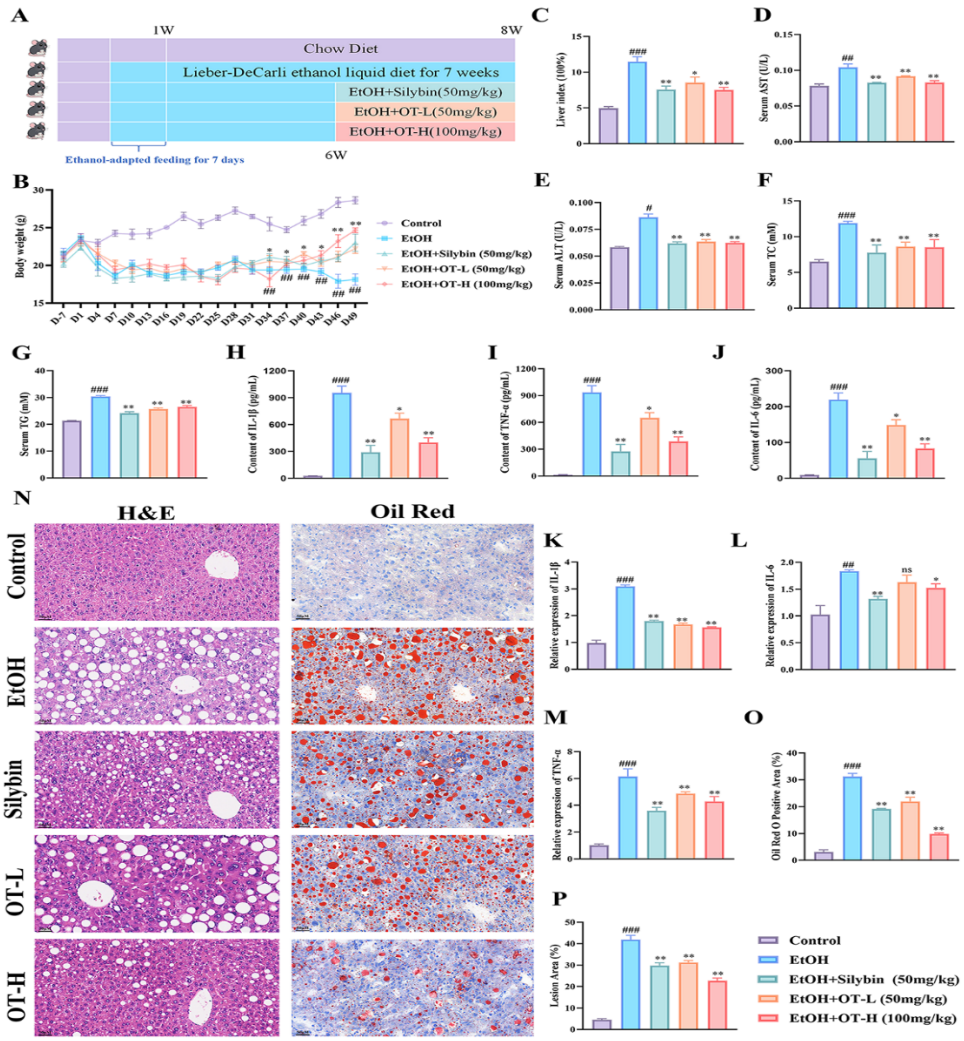


Figure 2. OT treatment effectively alleviated alcohol-induced liver damage. (A) The animal experimental protocol of this study. (B) Body weight changes in mice were monitored at 3-day intervals throughout the experimental period. (C) The liver to body weight ratio in mice after treatment with OT. (D,E) The serum AST and ALT activities after OT treatment. (F,G) The serum TG and TC activities after OT treatment. (H,I,J) The levels of cytokines IL-1β, TNF-α and IL-6 in serum from each group measured by ELISA. (K,L,M) The mRNA expression levels of IL-1β, IL-6 and TNF-α were measured by RT-PCR. (N) H&E and Oil Red O staining of mouse liver sections. (O,P) Histological scoring of Oil Red O and H&E stained liver sections in mice. Data are expressed as mean ± SD. Statistical significance was tested using one-way ANOVA. (*$P < 0.05$, **$P < 0.01$ compared to the model group; #$P < 0.05$, ##$P < 0.01$, ###$P < 0.001$ compared to the control group, n = 6).

Histological examination of liver tissues by H&E staining revealed that the ethanol-fed model group exhibited marked hepatocellular ballooning, inflammatory cell infiltration, and the presence of lipid vacuoles. These pathological features were significantly improved in mice treated with OT. Oil Red O staining further demonstrated extensive lipid droplet accumulation in the livers of ethanol-fed mice, indicating disrupted hepatic lipid metabolism induced by ethanol. Notably, OT administration substantially reduced hepatic lipid accumulation (Fig. 2N). These histopathological changes were consistent with semi-quantitative histological scoring (Fig. 2O-P). Importantly, the high-dose OT group (100 mg/kg) exhibited superior efficacy in improving ALD-related parameters compared to the positive control drug silybin, highlighting the strong therapeutic potential of OT in ALD management.

3.3. Proteomics analysis reveals potential targets of OT in the treatment of ALD

To further investigate the molecular mechanisms underlying the protective effects of OT in ALD, proteomic sequencing was performed on liver samples from each experimental group. Principal component analysis (PCA) based on the protein expression profiles revealed that the first and second principal components (PC1 and PC2) accounted for 52.9% and 17.1% of the total variance, respectively (Fig. 3A). The PCA score plot showed distinct separation among the control, model, and OT group, with the OT group exhibiting a protein expression pattern markedly different from that of the model group. DEP analysis identified 367 DEPs (208 downregulated and 159 upregulated) in the model group compared to the control group. In contrast, 208 DEPs (101 downregulated and 107 upregulated) were detected in the OT group relative to the model group (Fig. 3B). To illustrate the statistical significance of these changes, volcano plots were generated, displaying the DEPs in the control vs ethanol group (Fig. 3C) and OT group vs model group (Fig. 3D). Further analysis revealed that key proteins such as ORP8, ribosome biogenesis GTPase LSG1 (LSG1), and phosphatidylinositol 4-kinase type 2 alpha (PI4K2A) were significantly altered following ethanol exposure, and notably reversed by OT intervention. This suggests that OT may exert its therapeutic effects by modulating the expression of these pivotal proteins and their associated signaling pathways. A hierarchical clustering heatmap was constructed to visualize the distinct expression patterns of DEPs across different treatment groups (Fig. 3E). KEGG pathway enrichment analysis of DEPs between the OT and model groups revealed significant involvement of the AMPK and PPAR signaling pathways (Fig. 3F). Given their established importance in the pathogenesis of ALD, these pathways were selected for further validation in the subsequent experiments. Although other differentially expressed proteins, such as LSG1 and PI4K2A, may also be of potential interest, their mechanistic roles require further investigation in future studies.

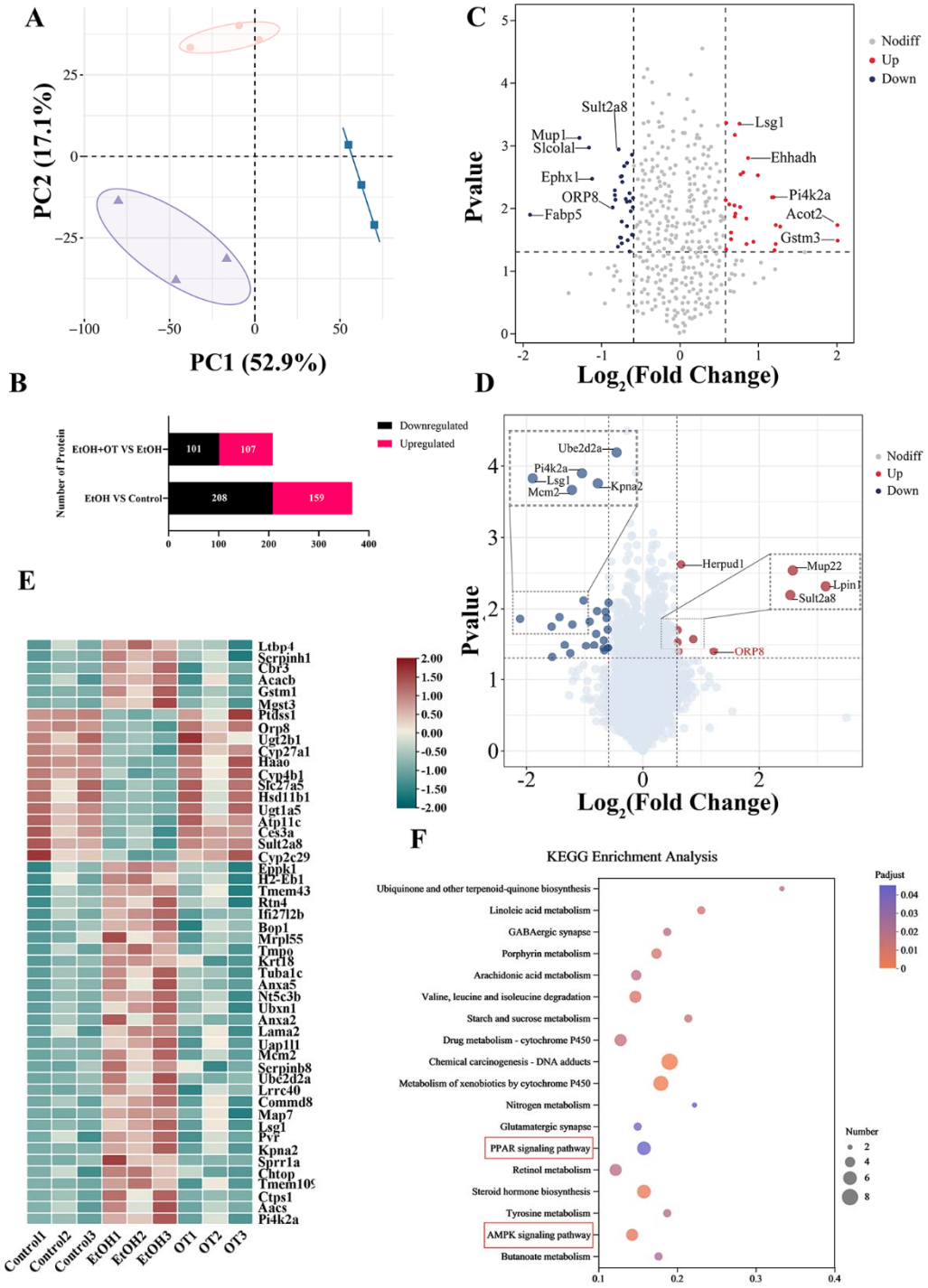


Figure 3. Identification of key targets reversed by OT in ALD mice via proteomics analysis. (A) PCA of samples from different experimental groups. (B) Bar chart showing the number of DEPs in each group. (C) Volcano plot showing differentially expressed proteins between the Control and Model groups. (D) Volcano plot showing differentially expressed proteins between the OT group and the Model group. (E) Heatmap analysis of protein expression profiles across different experimental groups. (F) KEGG enrichment bubble plot of differentially expressed proteins.

3.4. OT Alleviates ALD in Mice via the AMPK/SIRT1/PPARγ Pathway

To further elucidate the molecular mechanisms by which OT alleviates ALD, we performed immunofluorescence staining and Western blotting to assess the expression of lipid metabolism-related proteins in mouse liver tissues. IF analysis revealed that ethanol exposure markedly suppressed the hepatic expression of ORP8 compared to the control group, whereas OT treatment effectively restored ORP8 levels

(Fig. 4A). Western blotting analysis and quantitative scoring confirmed that OT significantly increased hepatic ORP8 expression in a dose-dependent manner (Fig. 4B-C), suggesting that OT may improve hepatic lipid metabolism via ORP8 regulation. Plin2, a constitutively expressed lipid droplet-associated protein, was substantially upregulated in ethanol-fed mice (Fig. 4D), and this upregulation was significantly suppressed by OT treatment, as verified by Western blotting and histological scoring (Fig. 4E-F). These findings collectively indicate that OT effectively reduces hepatic lipid droplet accumulation. In addition, IF staining of ATGL demonstrated that ethanol exposure induced ATGL overexpression, which was normalized following OT administration (Fig. 4G), consistent with the Western blot and scoring results (Fig. 4H-I).ORP8, Plin2, and ATGL are closely involved in hepatic lipid homeostasis and lipid droplet turnover. ORP8 is associated with intracellular lipid transport and lipophagy-related regulation, while Plin2 is a lipid droplet-associated protein widely recognized as a marker of lipid storage and steatosis. ATGL is a key enzyme responsible for triglyceride hydrolysis and lipid mobilization. Therefore, the OT-induced restoration of ORP8 expression, suppression of Plin2, and normalization of ATGL collectively suggest that OT alleviates alcohol-induced hepatic lipid metabolic disorder by improving lipid droplet dynamics and reducing excessive lipid accumulation.

To explore the core signaling mechanisms underlying the lipid-regulating and anti-inflammatory effects of OT, we examined key proteins in the AMPK/SIRT1/PPARγ signaling axis by Western blotting. Ethanol exposure disrupted adiponectin expression, thereby suppressing AMPK activation and impairing energy homeostasis. OT treatment significantly increased the hepatic p-AMPK/AMPK ratio, indicating effective restoration of AMPK signaling. AMPK inhibition resulted in insufficient SIRT1 activation, which led to hyperacetylation of PPARγ and downregulation of CPT1α, suggesting impaired mitochondrial β-oxidation. Concurrently, suppressed SIRT1 activity facilitated NF-κB activation and proinflammatory cytokine release, while inhibiting Nrf2 expression, indicating enhanced inflammation and reduced antioxidant capacity. OT treatment significantly decreased the hepatic p-NF-κB/NF-κB ratio and upregulated Nrf2 expression, demonstrating potent anti-inflammatory and antioxidant effects (Fig. 4J).

To validate these findings *in vitro*, an ALD cell model was established by co-stimulating HepG2 cells with FFA and ethanol. Western blotting revealed that ethanol and FFA stimulation suppressed adiponectin and AMPK activation, increased Plin2, and decreased ORP8 expression, all indicative of intracellular lipid accumulation and metabolic dysfunction. OT treatment reversed these pathological alterations (Fig. 5A-B). Inhibition of AMPK/SIRT1 signaling also impaired PPARγ and ATGL regulation and decreased CPT1α expression, further disrupting β-oxidation. Additionally, reduced SIRT1 activity enhanced NF-κB activation and suppressed Nrf2 expression, suggesting a proinflammatory and oxidative stress prone cellular state. Collectively, these results indicate that OT may exert protective effects against ALD by activating the AMPK/SIRT1 signaling axis, thereby modulating PPARγ-mediated lipid metabolism and restoring NF-κB/Nrf2 mediated inflammation and redox balance.

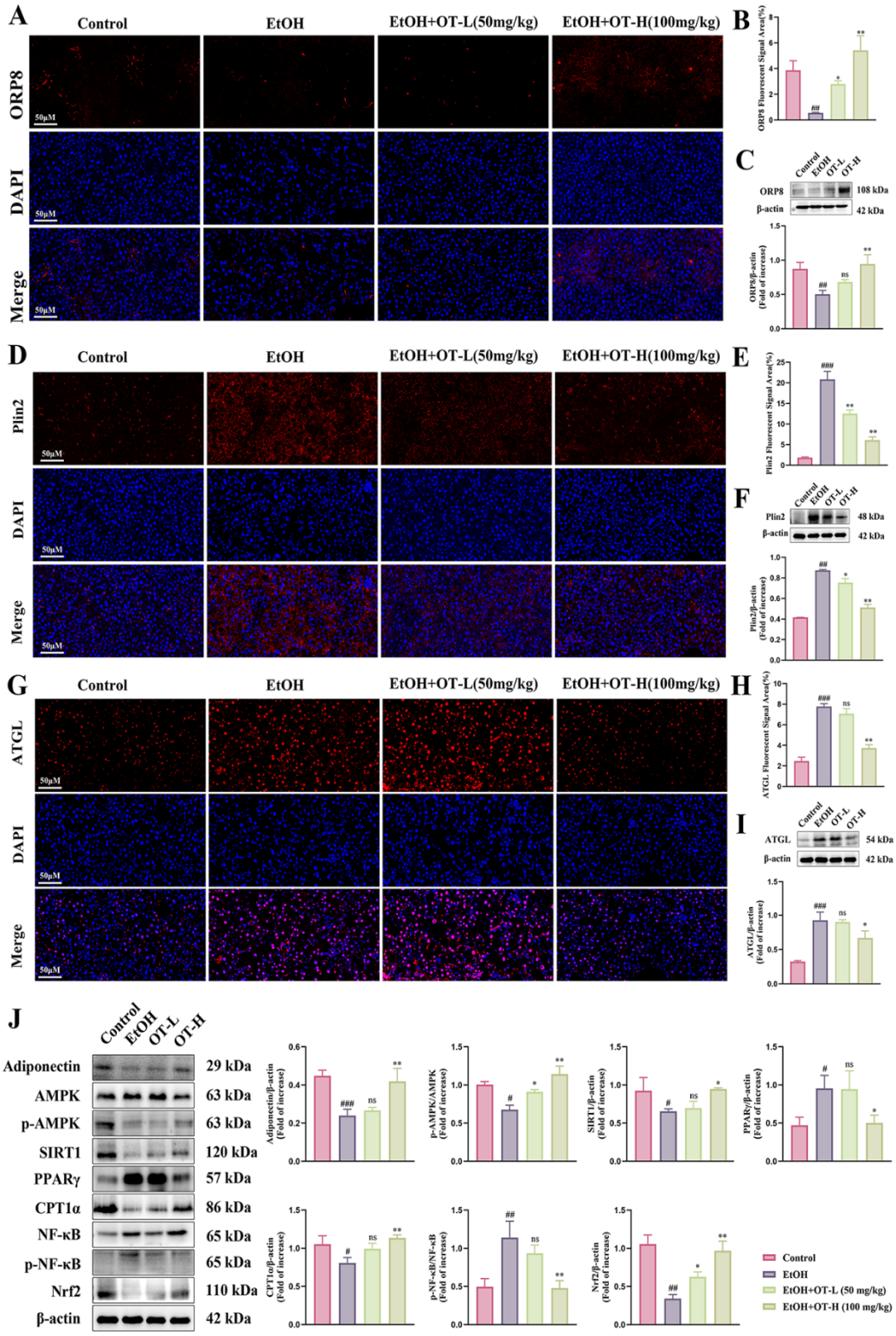


Figure 4. OT Alleviates ALD in Mice via the AMPK/SIRT1/PPARγ Pathway. (A,B) IF assay and statistics of ORP8. (C) Western blot analysis and quantification of ORP8 expression in mouse liver. (D,E) IF assay and statistics of Plin2. (F) Western blot analysis and quantification of Plin2 expression in mouse liver. (G,H) IF assay and statistics of ATGL. (I) Western blot analysis and quantification of ATGL expression in mouse liver. (J) Western blot analysis and quantification of Adiponectin, AMPK, p-AMPK, SIRT1, PPARγ, CPT1α, NF-κB, p-NF-κB, and Nrf2 protein expression in mouse liver tissue. Data are presented as mean ± SD. Statistical significance was assessed using one-way ANOVA. (*$P < 0.05$, **$P < 0.01$, compared with the model group; $^{\#}P < 0.05$, $^{\#\#}P < 0.01$, $^{\#\#\#}P < 0.001$ compared with the control group; ns: no statistical difference, n = 3).

To further validate the role of SIRT1 in the regulation of the AMPK/SIRT1/PPARγ signaling axis by OT, we conducted pharmacological inhibition experiments using the selective SIRT1 inhibitor EX-527. We first examined the effects of different concentrations of EX-527 on cell viability (Fig. S5U). As shown in Figures 5C–D, AMPK activation appeared unaffected by the inhibitor, and the OT-induced downregulation of SIRT1 and its downstream target PPARγ was significantly reversed upon co-administration of EX-527. Furthermore, SIRT1 inhibition abolished the inhibitory effect of OT on NF-κB activation, as evidenced by an increase in the p-NF-κB/NF-κB ratio. These findings indicate that the protective effects of OT on lipid metabolism and inflammatory responses depend, at least in part, on SIRT1 activation, further confirming the critical role of the AMPK/SIRT1/PPARγ signaling pathway in mediating the OT-induced hepatoprotective effects.

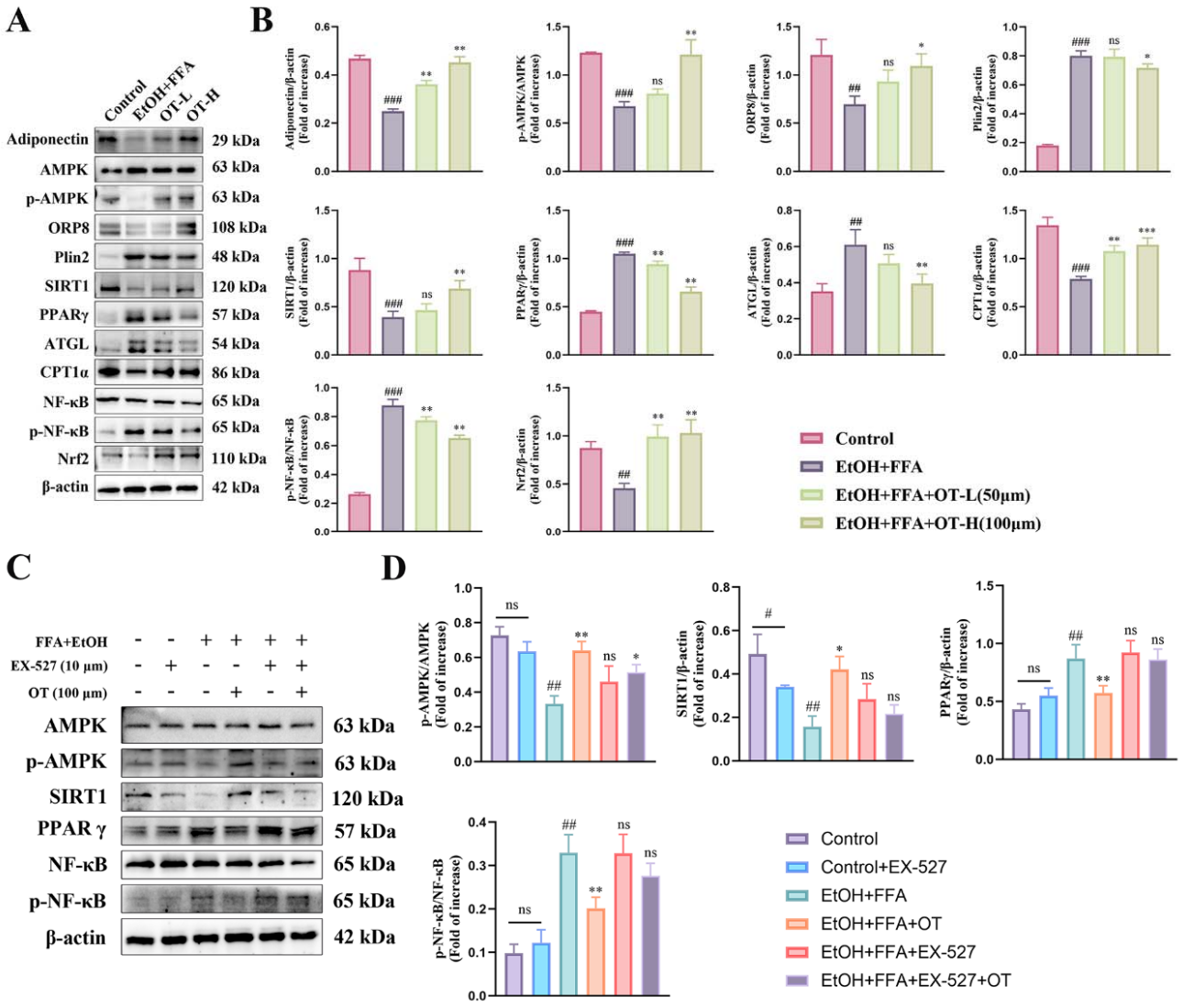


Figure 5. OT Alleviates ALD in Mice via the AMPK/SIRT1/PPARγ Pathway. (A,B) Western blot analysis and quantification of Adiponectin, AMPK, p-AMPK, ORP8, Plin2, SIRT1, PPARγ,ATGL, CPT1α, NF-κB, p-NF-κB, and Nrf2 protein expression in HepG2 Cells.(C,D) Western blot analysis and quantification of AMPK, p-AMPK, SIRT1, PPARγ, NF-κB, and p-NF-κB protein expression in HepG2 cells following the combined action of EX-527 and OT. Data are presented as mean ± SD. Statistical significance was assessed using one-way ANOVA. (*$P < 0.05$, **$P < 0.01$ compared to the model group; #$P < 0.05$, ##$P < 0.01$, ###$P < 0.001$ compared to the control group, n = 3)

3.5. OT alters the gut microbiota diversity

To evaluate the effect of OT on the intestinal microbiota, cecal and colonic contents from each group were collected, and bacterial DNA was extracted for 16S rRNA high-throughput sequencing. To minimize dimensionality distortion in β-diversity analysis, principal coordinates analysis (PCoA) was employed. PCoA results showed clear separation between control and model groups, while the OT group clustered closer to the control group than to the model group, indicating that OT partially restored the microbial community structure disrupted by ethanol exposure (Fig. 6C). Venn diagram analysis of amplicon sequence variants (ASVs) further illustrated the unique and shared ASVs among groups (Fig. 6B). To assess α-diversity, multiple indices were calculated, including observed richness, Shannon, Simpson, inverse Simpson, Chao1, and ACE. Generalized linear model (GLM) analysis showed consistent trends across indices: ethanol exposure significantly reduced all α-diversity indices compared to controls, while OT treatment significantly restored them, suggesting enhanced microbial richness and evenness after intervention (Fig. 6A). Microbial community composition was further examined at both phylum and genus levels. At the phylum level (Fig. 6D), the dominant phyla across all groups were Bacteroidota, Firmicutes, and Verrucomicrobiota, but their relative abundances differed significantly. In the control group, Bacteroidota (65.59%) and Firmicutes (24.59%) were predominant. model group increased Bacteroidota to 78.20% and decreased Firmicutes to 8.03%. OT treatment reversed this trend, reducing Bacteroidota to 71.61% and restoring Firmicutes to 22.03% (Fig. 6F). At the genus level (Fig. 6E), Muribaculaceae, Lachnospiraceae_unclassified, Lachnospiraceae_NK4A136_group, Akkermansia, and Alloprevotella were dominant across groups. Ethanol significantly reduced Lachnospiraceae related genera while enriching Muribaculaceae related genera (Fig. 6G), a dysbiosis pattern that was ameliorated by OT treatment. To further explore the impact of OT on ethanol-induced dysbiosis, comprehensive microbial profiling was performed. Ethanol exposure caused substantial alterations in gut microbiota composition at both phylum and genus levels, particularly affecting Firmicutes, Bacteroidota, and Actinobacteriota. OT administration, particularly at a high dose, significantly reversed the ethanol-induced gut microbiota dysbiosis, resulting in a microbial community structure that closely resembled that of the control group (Fig. 7A-B). Linear discriminant analysis (LDA) identified key discriminatory taxa reversed by OT treatment, including a reduction in pro-inflammatory genera such as *Prevotella* and *Odoribacter*, and enrichment of beneficial taxa such as *Ruminococcus* and *Oscillospirales* (Fig. 7C). These phylogenetic shifts were confirmed by cladogram analysis, which demonstrated the taxonomic distribution of significantly altered bacterial lineages across groups (Fig. 7D). Collectively, these results indicate that OT exerts a protective effect on gut microbiota diversity and composition, potentially contributing to its therapeutic efficacy against alcohol induced liver injury through modulation of the gut-liver axis. To further evaluate whether OT improves gut barrier integrity, the expression of intestinal tight junction proteins was examined by Western blotting(Fig. S2G). Ethanol exposure markedly reduced the expression of Occludin and ZO-1, whereas OT treatment significantly restored their levels. These findings suggest that OT

may protect against alcohol-induced intestinal barrier dysfunction, further supporting its beneficial role in regulating the gut-liver axis.

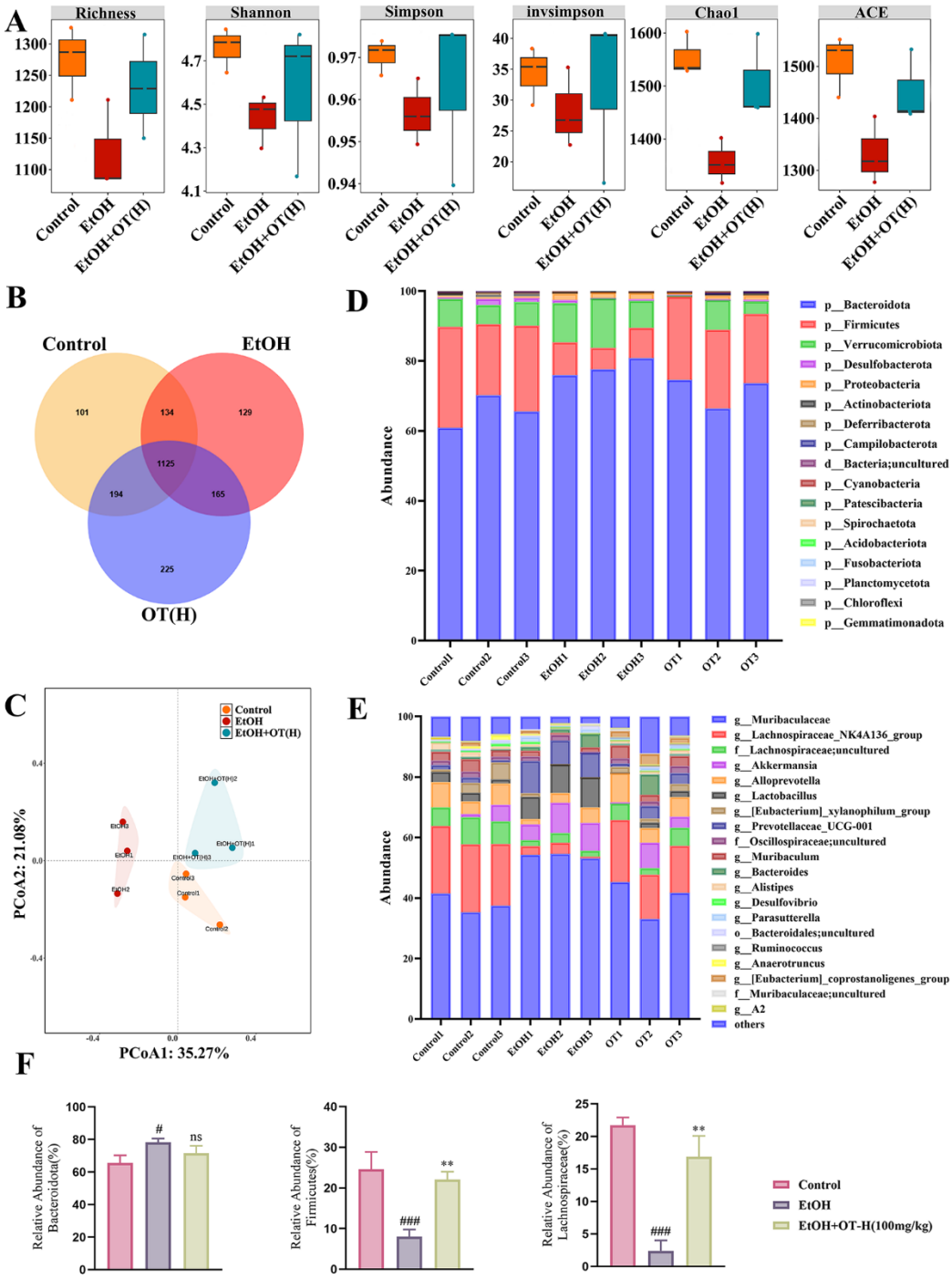


Figure 6. OT restores alcohol-induced gut microbiota dysbiosis. (A) Alpha diversity boxplot. (B) Venn diagram of ASVs among gut microbiota from different mouse groups. (C) PCoA of gut microbiota to evaluate beta diversity among groups. (D) Relative abundance of gut microbiota at the phylum level across different groups of experimental mice. (E) Relative abundance of gut microbiota at the genus level across different groups of experimental mice. (F) Relative abundance of the specific phylum in the two groups. Data are expressed as mean ± SD. Statistical significance was tested using one-way ANOVA. (*$P < 0.05$, **$P < 0.01$ compared to the model group; #$P < 0.05$, ##$P < 0.01$, ###$P < 0.001$ compared to the control group, n = 3)

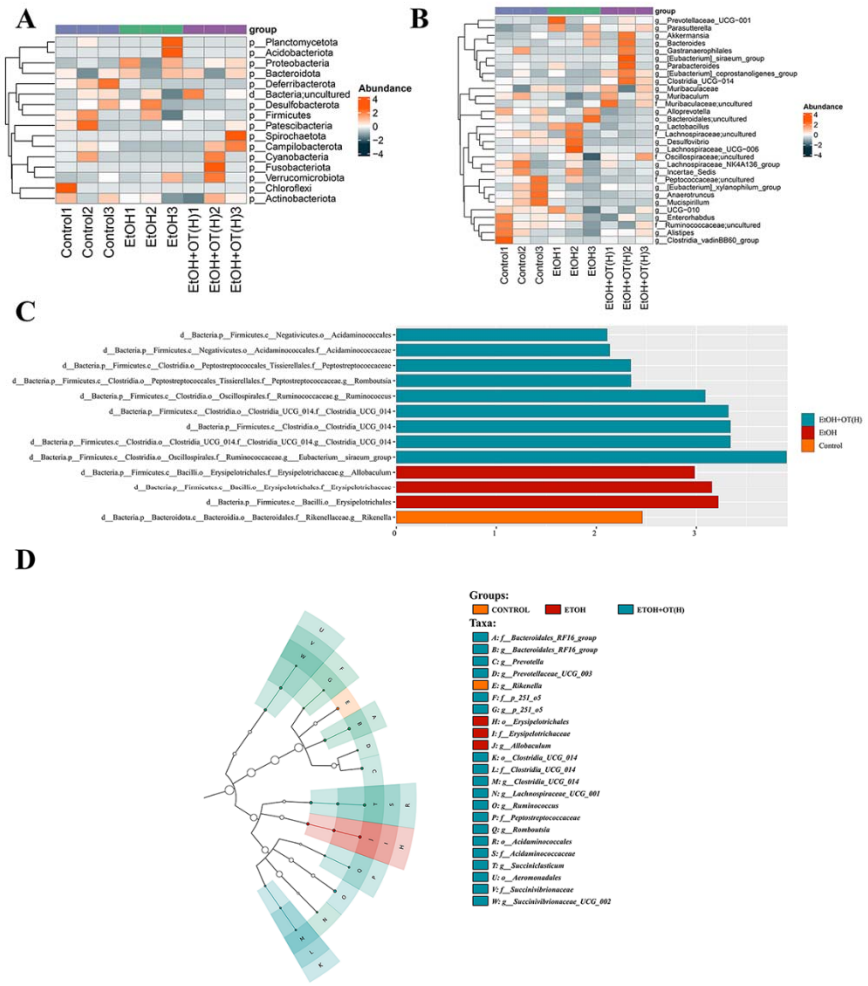


Figure 7. OT restores alcohol-induced gut microbiota dysbiosis. (A) Heatmap of differentially abundant bacterial phyla among experimental groups. (B) Heatmap of differentially abundant bacterial genera among experimental groups. (C,D) LDA score plot and phylogenetic tree of taxonomic features with differential abundance between groups.

3.6 OT treatment modulates metabolite SCFAs

OT intervention significantly altered the levels of SCFAs in the intestinal tract of mice with ALD. SCFAs, primarily produced through microbial fermentation of dietary fibers, play essential roles in maintaining intestinal homeostasis and have been increasingly recognized as a potential link between gut dysbiosis and ALD pathogenesis. Quantification of SCFAs in **cecal and colonic contents** showed that ethanol fed mice had significantly reduced levels of five major SCFAs (propionate, butyrate, valerate, acetate, and isobutyrate) compared to healthy controls, while the level of isovalerate was concurrently increased. Notably, OT administration effectively normalized these SCFAs levels, restoring them toward those observed in healthy controls (Fig. 8A-F). These findings suggest that OT may alleviate ALD-associated dysbiosis through the modulation of microbial metabolite output. Specifically, OT treatment led to a significant recovery of all six SCFAs, bringing their levels closer to those observed in the control group. To further investigate the relationship between gut microbiota and SCFAs production, Spearman's rank correlation analysis was performed, and p-values were adjusted using the Benjamini–Hochberg FDR method. At the phylum level, the relative abundance of *Verrucomicrobiota* was significantly negatively correlated with the levels of acetate and valerate (Fig. 8G). At the genus level, *Muribaculaceae* exhibited a strong negative

correlation with propionate levels, whereas *Lachnospiraceae_NK4A136_group* was positively correlated with both acetate and propionate concentrations. Moreover, butyrate levels showed a significant positive correlation with the abundance of *Alloprevotella* (Fig. 8H). Taken together, these results demonstrate that OT treatment can effectively restore SCFAs levels in ALD mice. The consistency between elevated SCFAs levels and increased abundance of key SCFAs producing genera (e.g., *Lachnospiraceae_NK4A136_group* and *Alloprevotella*) in OT treated mice further supports the therapeutic role of OT via reprogramming of gut microbial metabolism. To further evaluate whether SCFAs play a functional role in protecting against alcohol-induced liver injury, we conducted an exogenous supplementation experiment using NaB, a representative short-chain fatty acid. We first examined the effects of different concentrations of NaB on cell viability (Fig. S3E). As shown in Figure 8.I–K, NaB treatment significantly reduced elevated ALT, AST, and TG levels in an in vitro model of ALD, indicating that hepatocyte damage and lipid metabolism disorders were markedly alleviated. These results suggest that butyrate itself has a protective effect against alcohol-induced liver injury, thereby supporting the view that the restoration of SCFAs (especially butyrate) mediated by OT may contribute to its therapeutic efficacy.

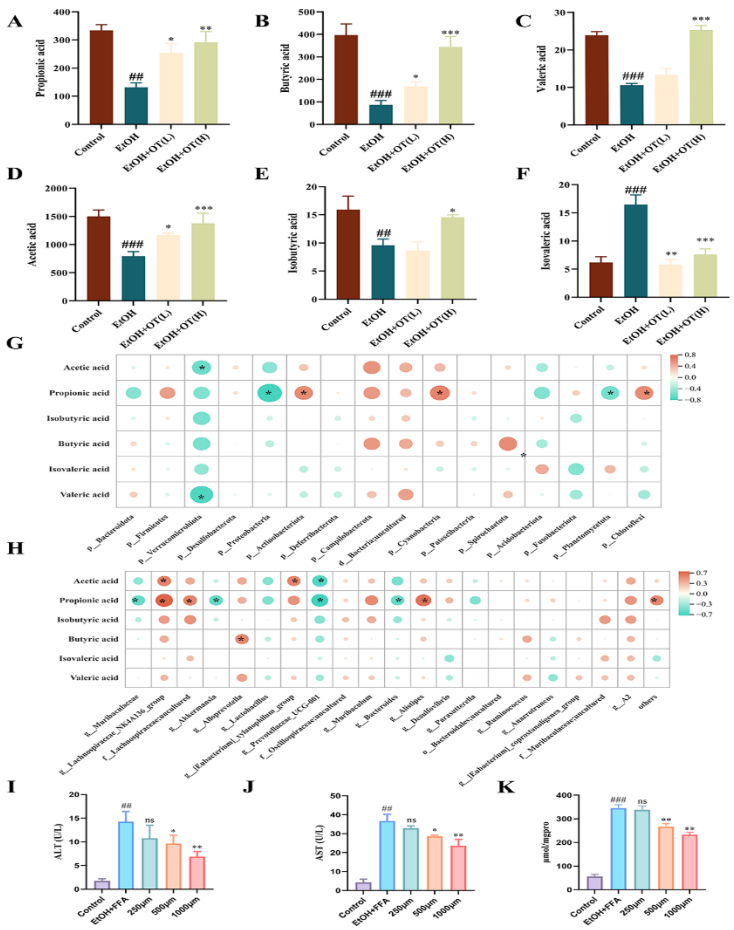


Figure 8. OT modulates the concentrations of SCFAs. (A-F) Concentrations of six SCFAs. (G,H) Spearman correlation heatmaps between SCFAs and gut microbiota at the phylum and genus levels across different groups. (I,J) The Effect of Sodium Butyrate Treatment on ALT and AST Activity in HepG2 Cells. (K) The Effect of Sodium Butyrate Treatment on TG Accumulation in HEpG2 Cells. Data are expressed as mean ± SD. Statistical significance was tested using one-way ANOVA. (*P < 0.05, **P < 0.01 ***P < 0.001 compared to the model group; #P < 0.05, ##P < 0.01, ###P < 0.001 compared to the control group, ns: no statistical difference, n = 3)

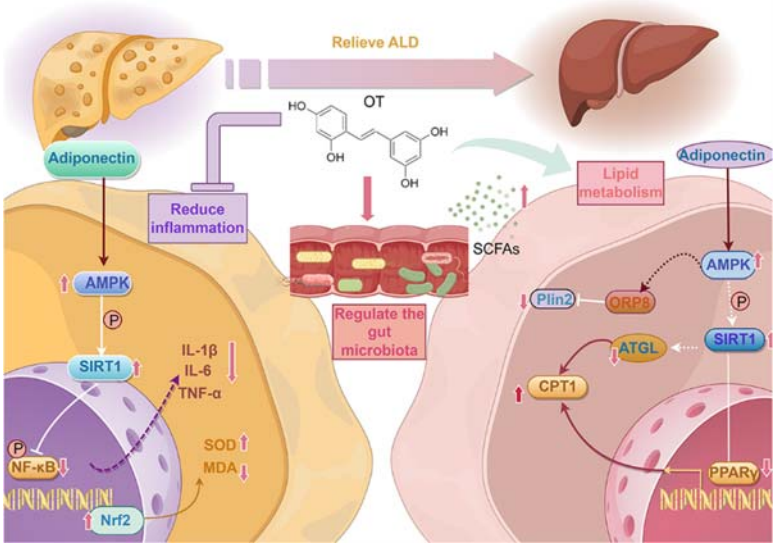


Figure 9. The mechanism diagram of OT reducing alcoholic liver injury by regulating lipid metabolism, inflammation.

4. Discussion

A central finding of our research is the pivotal role of the AMPK/SIRT1/PPARγ pathway in mediating OT's hepatoprotective effects. Proteomic analysis first pointed to AMPK and PPAR signaling as key targets, which was subsequently validated by Western blot and immunofluorescence assays. We demonstrated that OT treatment significantly enhanced the phosphorylation of AMPK and upregulated SIRT1 expression. This activation is critical, as AMPK serves as a master regulator of cellular energy homeostasis[28,29]. Its activation by OT likely counteracts the ethanol-induced suppression of fatty acid oxidation. Downstream, the upregulation of SIRT1 facilitated the deacetylation and functional activation of PPARγ, a nuclear receptor essential for lipid metabolism[30]. The consequent increase in CPT1α expression indicates a boost in mitochondrial β-oxidation, providing a mechanistic explanation for the reduced hepatic TG and TC levels observed in OT-treated mice[31].

Simultaneously, OT administration led to a significant decrease in the lipid droplet-associated protein Plin2 and an increase in ORP8 and ATGL. ALD is highly characterized by the excessive accumulation of lipid droplets (LDs) in hepatocytes. Plin2 acts as a protective shield on the surface of lipid droplets, preventing hydrolytic lipases from accessing neutral lipids. OT-induced downregulation of Plin2 effectively "uncoats" the lipid droplets. This structural exposure facilitates two simultaneous degradation pathways, it allows ATGL, the primary rate-limiting enzyme responsible for lipolysis, to access the lipid droplet surface to accelerate enzymatic breakdown, and it works synergistically with ORP8, a critical receptor for lipophagy that mediates the encapsulation and turnover of lipid droplets. Together, the modulation of the ORP8/Plin2/ATGL axis by OT severely accelerates the breakdown of accumulated triglycerides, fundamentally alleviating alcoholic hepatic steatosis[32,33]. This coordinated regulation of key hepatic proteins through the AMPK/SIRT1 axis represents a core mechanism by OT to reverse alcohol-induced metabolic dysfunction.

Beyond lipid metabolism, the AMPK/SIRT1 pathway is a well-known modulator of inflammation and oxidative stress. Our data show that OT treatment effectively suppressed the activation of the NF-κB pathway, as evidenced by a reduced p-NF-κB/NF-κB ratio. This suppression led to a marked decrease in the production of pro-inflammatory cytokines, including TNF-α, IL-1β, and IL-6, both in serum and liver tissue. The anti-inflammatory effect is likely attributable to SIRT1-mediated deacetylation of NF-κB, which dampens its transcriptional activity[34]. Indeed, our *in vitro* pharmacological inhibition experiments using the selective SIRT1 inhibitor EX-527 confirmed that the protective effects of OT on lipid metabolism and inflammatory responses are highly dependent on SIRT1 activation, thus functionally validating the causal necessity of the AMPK/SIRT1/PPARγ axis.

Furthermore, OT upregulated the expression of Nrf2, a master transcription factor governing the antioxidant response[35]. The activation of the Nrf2 pathway explains the observed increase in SOD activity and decrease in MDA levels, indicating a potentiation of the endogenous antioxidant defense system against alcohol-induced oxidative damage[36]. Therefore, OT orchestrates a dual anti-inflammatory and antioxidant response by concurrently modulating the NF-κB and Nrf2 pathways, creating a hepatic environment conducive to repair and recovery.

Our investigation extends the mechanism of OT beyond the liver to the gut, highlighting its role as a microbiota-modulating agent. 16S rRNA sequencing revealed that ethanol feeding caused severe dysbiosis, characterized by a decreased Firmicutes/Bacteroidota ratio and a loss of microbial diversity. OT intervention, particularly at the high dose, effectively reversed these alterations, shifting the microbial community structure back towards that of the healthy controls. Notably, OT enriched beneficial genera known for their SCFA-producing capacity, such as Lachnospiraceae_NK4A136_group and Alloprevotella. In particular, the enrichment of Lachnospiraceae may be biologically relevant to the improvement of the gut–liver axis. Recent studies have suggested that members of the Lachnospiraceae family are important butyrate-producing bacteria, and their enrichment has been associated with attenuation of liver injury. Oral fecal transplantation enriched gut Lachnospiraceae and increased butyrate levels, thereby mitigating acute liver injury[37]. In addition, Lachnospiraceae bacterium was significantly reduced in patients with ALD and in ethanol-fed mice, and that oral supplementation of this bacterium alleviated alcohol-induced liver injury[38]. These findings suggest that the enrichment of Lachnospiraceae observed in our study may contribute, at least in part, to hepatic protection through butyrate production and maintenance of intestinal homeostasis.

Crucially, this microbial remodeling was functionally consequential. We found that OT significantly restored the levels of major SCFAs, which were drastically depleted in the model group. SCFAs are not merely metabolic byproducts; they are potent signaling molecules. Butyrate and propionate, for instance, have been shown to enhance intestinal barrier integrity and exert anti-inflammatory effects systemically[39]. The strong positive correlation between the abundance of SCFA-producing bacteria (Lachnospiraceae_NK4A136_group) and the concentrations of SCFAs underscores a potential causal

relationship rather than mere coincidence. To confirm the functional role of SCFAs, our additional in vitro experiments demonstrated that exogenous sodium butyrate directly alleviated hepatocellular injury and lipid accumulation in the ALD cell model. Furthermore, to provide direct evidence for intestinal barrier repair, we showed that OT treatment significantly restored the expression of intestinal tight junction proteins ZO-1 and Occludin, which were disrupted by ethanol exposure. By repairing the intestinal barrier, OT likely limits the translocation of endotoxins like LPS, thereby mitigating the persistent low-grade inflammation that fuels liver injury. These findings position the improvement of gut microbiota and its metabolites as an important upstream regulatory factor in OT's protective mechanism.

5. Conclusion

This study conclusively demonstrates that OT confers significant protection against ALD through direct activation of the hepatic AMPK/SIRT1 signaling pathway and the beneficial remodeling of the gut microbiota. At the hepatic core, OT directly activates the AMPK/SIRT1/PPARγ signaling pathway, which fundamentally mitigates hepatic steatosis by accelerating lipid droplet turnover via the ORP8/Plin2/ATGL axis, while concurrently alleviating inflammation and oxidative stress through the NF-κB and Nrf2 pathways. Concurrently in the gut, OT intervention restores ethanol-induced microbial dysbiosis, particularly by enriching SCFA-producing bacteria such as Lachnospiraceae. The consequent elevation of SCFAs significantly reinforces intestinal barrier integrity by restoring tight junction proteins, thereby preventing gut-derived endotoxin translocation. These gut-mediated improvements synergize with the direct hepatic signaling regulation, creating a positive therapeutic loop. Although future investigations are warranted to precisely trace inter-organ metabolite trafficking via the portal vein, our findings provide robust evidence that OT is a promising, multi-target therapeutic candidate for ALD and offer fresh mechanistic insights into pharmacological interventions targeting gut-liver crosstalk.

Acknowledgments

This work was supported by the National Natural Science Foundation of China (82505006), the Natural Science Foundation of Hubei Province, China (No. 2023AFD118), HBUCM Scientific & Technological Innovation Project (2024KJCX006), Project of Hubei Province Traditional Chinese Medicine Innovation Team (ZY2025J002), and HBUCM Key Scientific Research Projects for the Construction of "Double First-Class" (Outstanding Youth Foundation). We sincerely thank Prof. Hongtao Bi (NWIPB, CAS) for his invaluable assistance with the animal tests and data analysis.

Data Availability Statement

All data generated or analyzed during this study are included in this published article and its supplementary information files.

Conflict of Interest

The authors declare no competing interests.

References

[1] Luo, Q., Qiu, J., Chen, M., Yang, N., Li, X., Huang, S., Ma, Q., Li, Z., Lou, D., Du, Y., Chen, L., Shen, Q., Chen, F., Li, C., & Qiu, P. (2025). Vine tea (Ampelopsis grossedentata) ameliorates chronic alcohol-induced hepatic steatosis, oxidative stress, and inflammation via YTHDF2/PGC-1α/SIRT3 axis. Food Research International, 209, 116321. https://doi.org/10.1016/j.foodres. 2025.116321.

[2] Wang, X., Sun, Z., Wang, X., Li, M., Zhou, B., & Zhang, X. (2024). Solanum nigrum L. berries extract ameliorated the alcoholic liver injury by regulating gut microbiota, lipid metabolism, inflammation, and oxidative stress. Food Research International, 188, 114489. https://doi.org/10.1016/j.foodres.2024.114489.

[3] Prince, D. S., Nash, E., & Liu, K. (2023). Alcohol-Associated Liver Disease: Evolving Concepts and Treatments. Drugs, 83(16), 1459-1474. https://doi. Org/1 0.1007/s40265-023-01939-9.

[4] Singal, A. K., & Mathurin, P. (2021). Diagnosis and Treatment of Al cohol-A ssociated Liver Disease. JAMA, 326(2), 165. https://doi.org/10.1016/j.foodres. 2024.114489.

[5] Hao, S., Lv, Y., Wang, Y., Liu, K., Yu, X., & Tan, M. (2025). Potential benefits of orally deliverable silymarin-loaded spirulina platensis in mitigating alcoholic liver disease. Food Research International, 212, 116508. https://doi.org/10.1016 /j.foodres.2025.116508.

[6] Kumar, A., Paliwal, R., & Gulbake, A. (2023). Lentinan: An unexplored novel biomaterial in drug and gene delivery applications. Journal of Controlled Release, 356, 316-336. https://doi.org/10.1016/j.jconrel.2023.02.034.

[7] Pan, M.-H., Koh, Y.-C., Lee, T.-L., Wang, B., Chen, W.-K., Nagabhushanam, K., & Ho, C.-T. (2019). Resveratrol and Oxyresveratrol Activate Thermogenesis via Different Transcriptional Coactivators in High-Fat Diet-Induced Obese Mice. Journal of Agricultural and Food Chemistry, 67(49), 13605-13616. https://doi. org/10.1021/acs.jafc.9b05963.

[8] Song, W., Wang, H.-J., Bucheli, P., Zhang, P.-F., Wei, D.-Z., & Lu, Y.-H. (2009). Phytochemical Profiles of Different Mulberry (Morus sp.) Species from China. Journal of Agricultural and Food Chemistry, 57(19), 9133-9140. https://doi. Org/ 10.1021/jf9022228.

[9] Likhitwitayawuid, Kittisak. 2021. “Oxyresveratrol: Sources, Productions, Biological Activities, Pharmacokinetics, and Delivery Systems.” Molecules 26(14):4212. doi:10.3390/molecules26144212.

[10] Choi, H. Y., Lee, J.-H., Jegal, K. H., Cho, I. J., Kim, Y. W., & Kim, S. C. (2016). Oxyresveratrol abrogates oxidative stress by activating ERK-Nrf2 pathway in the liver. Chemico-Biological Interactions, 245, 110-121. https://doi.org/10.1016/j.c bi.2015.06.024.

[11] Liu, Y., Ren, W., Bai, Y., Wan, L., Sun, X., Liu, Y., Xiong, W., Zhang, Y.-Y., & Zhou, L. (2018). Oxyresveratrol prevents murine H22 hepatocellular carcinoma growth and lymph node metastasis via inhibiting tumor angiogenesis and lymphangiogenesis. Journal of Natural Medicines, 72(2), 481-492. https://doi.Or g/10.1007/s11418-018-1173-2.

[12] Wang, L., Zhao, H., Wang, L., Tao, Y., Du, G., Guan, W., Liu, J., Brennan, C., Ho, C.-T., & Li, S. (2020). Effects of Selected Resveratrol Analogues on Activation and Polarization of Lipopolysaccharide-Stimulated BV-2 Microglial Cells. Journal of Agricultural and Food Chemistry, 68(12), 3750-3757. https://doi.org/ 10.1021/acs.jafc.0c00498.

[13] Yang, G., Zhan, J., Yang, Y., Yuan, L., Wang, P., Ho, C.-T., & Li, S. (2021). Inhi bitory effects of oxyresveratrol on ERK and Smad1/2 phosphorylation and HSC activation in preventing carbon tetrachloride-induced rat liver fibrosis. Food Science and Human Wellness, 10(1), 6-12. https://doi.org/10.1016/j.fshw.2020. 08.007.

[14] Shi, X., Xu, L., Zhang, J., Mo, J., Zhuang, P., & Zheng, L. (2023). Oxyresveratr ol from mulberry branch extract protects HUVECs against oxidized Low-density Lipoprotein-induced oxidative injury via activation of the Nrf-2/HO-1 pathway. Journal of Functional Foods, 100, 105371. https://doi.org/10.1016/j.jff.2022.105 371.

[15] Zhuge, A., Li, S., Han, S., Yuan, Y., Shen, J., Wu, W., Wang, K., Xia, J., Wang, Q., Gu, Y., Chen, E., & Li, L. (2025). Akkermansia muciniphila-derived acetate activates the hepatic AMPK/SIRT1/PGC-1α axis to alleviate ferroptosis in metabolic-associated fatty liver disease. Acta Pharmaceutica Sinica B, 15(1), 151-167. https://doi.org/10.1016/j.apsb.2024.10.010.

[16] Zhao L, Duan Y, Li Z, Li J, Li S. Unearthing the Potential Therapeutic Effects of Oxyresveratrol Based on Intrinsic Links between Pharmacological Effects: Implications for the Gut-Liver-Brain Axis. Pharmaceuticals. 2024; 17(8):1063. https://doi.org/10.3390/ph17081063.

[17] Li, Q., Tan, J.-X., He, Y., Bai, F., Li, S.-W., Hou, Y.-W., Ji, L.-S., Gao, Y.-T., Zh ang, X., Zhou, Z.-H., Yu, Z., Fang, M., Gao, Y.-Q., & Li, M. (2022). Atractylenolide III ameliorates Non-Alcoholic Fatty Liver Disease by activating Hepatic Adiponectin Receptor 1-Mediated AMPK Pathway. International Journal of Biological Sciences, 18(4), 1594-1611. https://doi.org/10.7150/ijbs.68873.

[18] Zhu, L., Xu, J.-J., Li, H.-D., Li, J.-J., Cheng, M., Niu, X.-N., Jia, P.-C., Liu, J.-Y., Huang, C., Lv, X.-W., & Li, J. (2023). Berberine Ameliorates Abnormal Lipid Metabolism via the Adenosine Monophosphate-Activated Protein Kinase/Sirtuin 1 Pathway in Alcohol-Related Liver Disease. Laboratory Investigation, 103(4), 100041. https://doi.org/10.1016/j.labinv.2022.100041.

[19] Jiang, M., Feng, Y., Wang, J. et al. Saikogenin A improves ethanol-induced liver injury by targeting SIRT1 to modulate lipid metabolism. Commun Biol 7, 1547 (2024). https://doi.org/10.1038/s42003-024-07234-x

[20] Tian, D., Zhong, X., Fu, L., Zhu, W., Liu, X., Wu, Z., Li, Y., Li, X., Li, X., Tao, X., Wei, Q., Yang, X., & Huang, Y. (2022). Therapeutic effect and mechanism of polysaccharides from Anoectochilus Roxburghii (Wall.) Lindl. in diet-induced obesity. Phytomedicine, 99, 154031. https://doi.org/10.1016/j.phymed.2022.154 031.

[21] Cantó C, Jiang LQ, Deshmukh AS, Mataki C, Coste A, Lagouge M, Zierath JR, Auwerx J. Interdependence of AMPK and SIRT1 for metabolic adaptation to fasting and exercise in skeletal muscle. Cell Metab. 2010 Mar 3;11(3):213-9. doi: 10.1016/j.cmet.2010.02.006.

[22] Choi, Y. H., Bae, J. K., Chae, H.-S., Kim, Y.-M., Sreymom, Y., Han, L., Jang, H. Y., & Chin, Y.-W. (2015). α-Mangostin Regulates Hepatic Steatosis and Obesity through SirT1-AMPK and PPARγ Pathways in High-Fat Diet-Induced Obese Mice. Journal of Agricultural and Food Chemistry, 63(38), 8399-8406. https://doi.org/10.1021/acs.jafc.5b01637.

[23] Hsu, C. L., & Schnabl, B. (2023). The gut-liver axis and gut microbiota in health and liver disease. Nature Reviews Microbiology, 21(11), 719-733. https://doi.org /10.1038/s41579-023-00904-3.

[24] Lang, S., & Schnabl, B. (2020). Microbiota and Fatty Liver Disease-the Known, the Unknown, and the Future. Cell Host & Microbe, 28(2), 233-244. https://doi.org/10.1016/j.chom.2020.07.007.

[25] Mukhopadhya I, Louis P. Gut microbiota-derived short-chain fatty acids and their role in human health and disease. Nat Rev Microbiol. 2025 Oct;23(10):635-651. doi: 10.1038/s41579-025-01183-w.

[26] Li, Q., Liu, W., Zhang, H., Chen, C., Liu, R., Hou, H., Luo, Q., Yu, Q., Ouyang, H., Feng, Y., & Zhu, W. (2023). α-D-1,3-glucan from Radix Puerariae thomsonii improves NAFLD by regulating the intestinal flora and metabolites. Carbohydrate Polymers, 299, 120197. https://doi.org/10.1016/j.carbpol.2022.12 0197.

[27] Wang, W., Zhao, X., Ma, Y., Zhang, J., Xu, C., Ma, J., Hussain, M. A., Hou, J., & Qian, S. (2023). Alleviating Effect of Lacticaseibacillus rhamnosus 1.0320 Combined with Dihydromyricetin on Acute Alcohol Exposure-Induced Hepatic Impairment: Based on Short-Chain Fatty Acids and Adenosine 5′-Monophosph ate-Activated Protein Kinase-Mediated Lipid Metabolism Signaling Pathway. Journal of Agricultural and Food Chemistry, 71(12), 4837-4 850. http s://doi.org/10.1021/acs.jafc.2c08523.

[28] Li, N., Yin, L., Shang, J., Liang, M., Liu, Z., Yang, H., Qiang, G., Du, G., & Yang, X. (2023). Kaempferol attenuates nonalcoholic fatty liver disease in type 2 diabetic mice via the Sirt1/AMPK signaling pathway. Biomedicine & Pharmacotherapy, 165, 115113. https://doi.org/10.1016/j.biopha.2023.115113.

[29] You, M., Jogasuria, A., Taylor, C., & Wu, J. (2015). Sirtuin 1 signaling and alcoh olic fatty liver disease. Hepatobiliary Surgery and Nutrition, 4(2), 88-100. http://dx.doi.org/10.3978/j.issn.2304-3881.

[30] Qiang, L., Wang, L., Kon, N., Zhao, W., Lee, S., Zhang, Y., Rosenbaum, M., Zh ao, Y., Gu, W., Farmer, S. R., & Accili, D. (2012). Brown Remodeling of White Adipose Tissue by SirT1-Dependent Deacetylation of Pparγ. Cell, 150(3), 620-632. https://doi.org/10.1016/j.cell.2012.06.027.

[31] Helsley RN, Park SH, Vekaria HJ, Sullivan PG, Conroy LR, Sun RC, Romero MDM, Herrero L, Bons J, King CD, Rose J, Meyer JG, Schilling B, Kahn CR, Softic S. Ketohexokinase-C regulates global protein acetylation to decrease carnitine palmitoyltransferase 1a-mediated fatty acid oxidation. J Hepatol. 2023 Jul;79(1):25-42. doi: 10.1016/j.jhep.2023.02.010. Epub 2023 Feb 21.

[32] Guyard, V., Monteiro-Cardoso, V. F., Omrane, M., Sauvanet, C., Houcine, A., B oulogne, C., Ben Mbarek, K., Vitale, N., Faklaris, O., El Khallouki, N., Thiam, A. R., & Giordano, F. (2022). ORP5 and ORP8 orchestrate lipid droplet biogenesis and maintenance at ER-mitochondria contact sites. Journal of Cell Biology, 221(9). https://doi.org/10.1083/jcb.202112107.

[33] Pu, M., Zheng, W., Zhang, H., Wan, W., Peng, C., Chen, X., Liu, X., Xu, Z., Zh o u, T., Sun, Q., Neculai, D., & Liu, W. (2023). ORP8 acts as a lipophagy receptor to mediate lipid droplet turnover. Protein & Cell, 14(9), 653-667. https://doi.Org /10.1093/procel/pwac063.

[34] Zhou, Y., Wang, S., Wan, T., Huang, Y., Pang, N., Jiang, X., Gu, Y., Zhang, Z., Luo, J., & Yang, L. (2020). Cyanidin-3-O-β-glucoside inactivates NLRP3 inflammasome and alleviates alcoholic steatohepatitis via SirT1/NF-κB signaling pathway. Free Radical Biology and Medicine, 160, 334-341. https://doi.org/10. 1016/j.freeradbiomed.2020.08.006.

[35] Fuertes-Agudo M, Luque-Tévar M, Cucarella C, Martín-Sanz P, Casado M. Advances in Understanding the Role of NRF2 in Liver Pathophysiology and Its Relationship with Hepatic-Specific Cyclooxygenase-2 Expression. Antioxidants (Basel). 2023 Jul 26;12(8):1491. doi: 10.3390/antiox12081491.

[36] Yang, R., Song, C., Chen, J., Zhou, L., Jiang, X., Cao, X., Sun, Y., & Zhang, Q. (2020). Limonin ameliorates acetaminophen-induced hepatotoxicity by activating Nrf2 antioxidative pathway and inhibiting NF-κB inflammatory response via upregulating Sirt1. Phytomedicine, 69, 153211. https://doi.Org/1 0.1016/j.phymed.2020.153211.

[37] Yang, C.-J., Chang, H.-C., Sung, P.-C., Ge, M.-C., Tang, H.-Y., Cheng, M.-L., Cheng, H.-T., Chou, H.-H., Lin, C.-Y., Lin, W.-R., Lee, Y.-S., & Hsieh, S.-Y. (2024). Oral fecal transplantation enriches lachnospiraceae and butyrate to mitigate acute liver injury. Cell Reports, 43(1), 113591. https://doi.org/10.1016/j.celrep.2023.113591

[38] Zhang, H., Hu, Q., Zhang, Y., Yang, L., Tian, S., Zhang, X., Shen, H., Shu, H., Xie, L., Wu, D., Zhou, L., Wei, X., Cheng, C., Jiang, J., Wang, H., Shen, C., Kong, D., & Xu, L. (2025). Lachnospiraceae bacterium alleviates alcohol-associated liver disease by enhancing N-acetyl-glutamic acid levels and inhibiting ferroptosis through the KEAP1-NRF2 pathway. Gut Microbes, 17(1), 2517821. https://doi.org/10.1080/19490976.2025.2517821

[39] Lee, J.-E., Ha, J. S., Park, H.-Y., & Lee, E. (2020). Alteration of gut microbiota composition by short-term low-dose alcohol intake is restored by fermented rice liquor in mice. Food Research International, 128, 108800. https://doi.org/10.101 6/j.foodres.2019.108800.